Article:

Population-Inversion and Gain Estimates for a Semiconductor TASER

P. Harrison, *Senior Member, IEEE,* and R. A. Soref, *Senior Member, IEEE*

Abstract—We have investigated a solid-state design advanced (see Soref et al. in SPIE Proceedings, vol. 3795, p. 516 , 1999) to achieve a terahertz-amplification-by-the-stimulated-emission-of-radiation (TASER). The original design was based on light-to heavy-hole intersubband transitions in SiGe/Si heterostructures. This work adapts the design to electron intersubband transitions in the more readily available GaAs/Ga$_{1-x}$Al$_x$As material system. It is found that the electric-field induced anti-crossings of the states, derived from the first excited state with the ground states of a superlattice in the Stark-ladder regime, offers the possibility of a population inversion and gain at room temperature.

Index Terms—Far-infrared, intersubband, quantum cascade lasers, Stark-ladder, superlattice, terahertz.

I. INTRODUCTION

THE REALIZATION of a solid-state coherent source of Terahertz radiation, a terahertz-amplification-by-the-stimulated-emission-of-radiation (TASER) [1] is becoming an increasingly important focus of the semiconductor research community. In particular, there has been a recent flurry of activity on both the theoretical [2]–[5] and experimental [6]–[8] fronts. In this vein, Soref *et al.* [9] proposed a device design based on the philosophy of light-hole-to-heavy-hole intersubband transitions within a p-type SiGe/Si superlattice. A bias applied to the superlattice was used to align the heavy-hole subband of well n with the light-hole subband of well $n + 1$. The result is a "quantum staircase" arrangement, a more complex manifestation of the single Stark-ladder tunable far-infrared emitter proposed by Donovan *et al.* [10].

In this work, the p-type TASER proposed by Soref *et al.* is adapted for realization in the more readily available GaAs/Ga$_{1-x}$Al$_x$As material system, and in this form the design is a particular manifestation of the idea originally proposed by Kazarinov and Suris [11]. Quantum cascade lasers based on electron transitions in n-type GaAs/Ga$_{1-x}$Al$_x$As have been demonstrated by several groups, for example [12], [13], and hence at this moment in time, it offers a quicker route to the realization of a device than p-type SiGe/Si heterostructures. Clearly, there are no light- and heavy-hole subbands in an n-type device and so the required subband structure is created by making use of subbands derived from the lowest two conduction minibands in a superlattice.

II. THE DESIGN PROCESS

Two basic criteria have to be met in deciding on the basic material parameters of the superlattice. Firstly, the basic operating principle requires two subbands within each quantum well, and secondly the energy separation of these subbands must be within the terahertz (4–41 meV) region of the spectrum. With this aim, a series of calculations were performed on a single GaAs quantum well surrounded by Ga$_{1-x}$Al$_x$As barriers. It was found that quantum well widths greater than 200 Å satisfied both of the above criteria. In addition, on constructing the superlattice, reasonable interaction between the states of neighboring quantum wells was required; hence, the relatively low barrier height given by the Al concentration of 10% was settled upon. In addition, the barrier width of 60 Å was chosen.

In order to make the calculations tractable, just three periods of the superlattice were included in the theoretical model. This is sufficient to demonstrate all the design and operating principles and to represent the eigenstates of the electrons accurately. In reality, more periods of the superlattice would be used to make use of the "carrier-recycling" advantages of the quantum cascade principle.

III. TASER OPERATING PRINCIPLES

As mentioned above, the mode of operation of the proposed device differs from the original proposal [9] in that two conduction minibands are used as a source for the field-split subbands rather than light- and heavy-hole minibands. The mode of operation can be understood by considering the wave functions of the $k = 0$ subband minima as plotted in Fig. 1 in conjunction with their $k = 0$ energies as a function of the applied electric field, as illustrated in Fig. 2.

Finite-length superlattices do not have a miniband, but rather a collection of closely spaced eigenstates. In this example of three quantum wells, then the lowest "miniband" is actually three electron energy levels. This is illustrated in the low-field plot of the wave functions in Fig. 1(a). In addition, this quantum well system has been designed to have a higher energy "miniband" too, and this manifests itself as the three closely spaced energy levels between 24–26 meV.

Fig. 2 illustrates the behavior of the energy levels as a function of the field. Increasing the applied electric field from zero moves the system into the Stark-ladder regime, with equal-spaced energy levels, the spacing itself being proportional to the field. With the origin for the electric-field potential
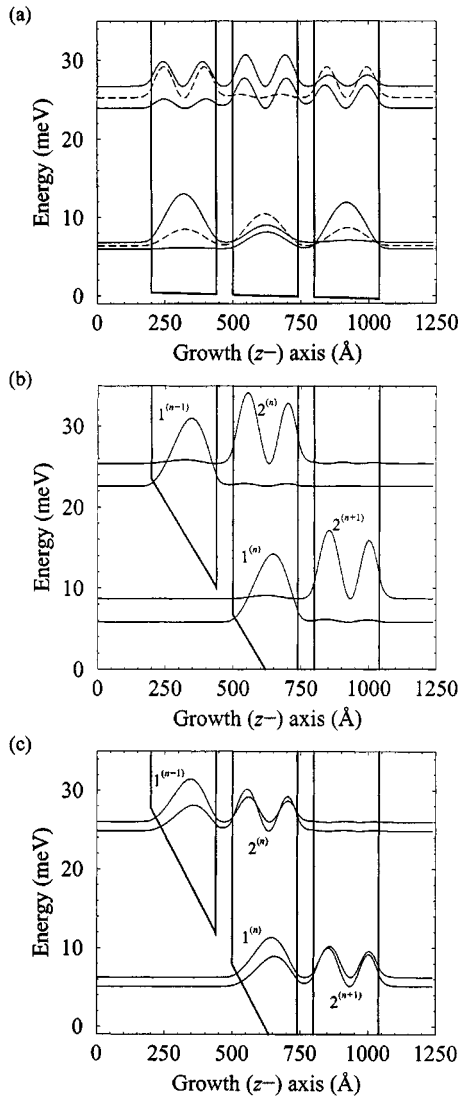
Fig. 1. Conduction band electron wave functions of the electric-field strengths of 0.1 (low field), 5.6 (just before the anti-crossing), and 6.6 (just after the anti-crossing) kilovolt per centimeter.
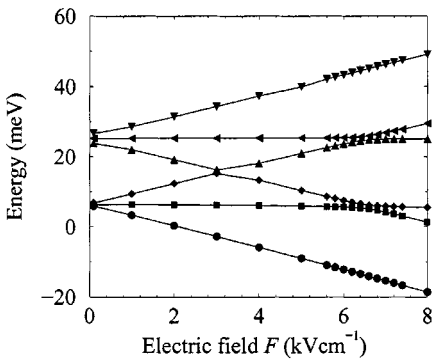

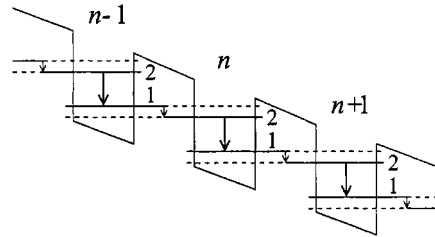Fig. 2. Subband minima as a function of the electric field.

Fig. 3. Lasing level structure derives from two levels (denoted by two solid lines) which originate from one particular well. As the electric field is increased from zero, the ground state (level 1) in well n eventually is tuned to the same energy as the first excited state in well $n + 1$. The diagram shows the situation just beyond this anti-crossing: solid lines show where the state originates from, and dashed lines show where the state extends to around the anti-crossing.

device proposal) that states from the upper miniband begin to overlap with states from the lower miniband. The first of these features occurs around 3 kVcm^{-1} (see Fig. 2). The higher level (by this field) localized in the right-hand well undergoes an anti-crossing with the lower level localized in the left-hand well. Fig. 1(b) illustrates the wave functions of the second, third, fourth and fifth highest energy levels after this point, at a field of 5.6 kVcm^{-1}. It can be seen from Fig. 1(b) that the state originating from the upper miniband, now localized in the right-hand well ($|2^{(n+1)}\rangle$) is decreasing in energy and approaching the state originating from the lower miniband, now localized in the central well ($|1^{(n)}\rangle$). Thus, further increases in the electric field make a second anti-crossing inevitable and this, indeed, occurs at field around 6.4 kVcm^{-1} (see Fig. 2). Note that two anti-crossings occur simultaneously; this represents the point where *all* the states originating from the upper miniband which are now localized in well $n + 1$, say, interact with the states originating in the lower miniband which are now localized in well n (numbering the wells from left to right).

Fig. 1(c) illustrates the same wave functions as in Fig. 1(b) just beyond this second anti-crossing at 6.6 kVcm^{-1}. This is the electric-field point at which the expected device operation is expected to begin. Electrons in any of the levels equivalent to the third-highest energy state ($|2^{(n)}\rangle$) in Fig. 1(c), can scatter to the upper ($|1^{(n)}\rangle$) (or indeed the lower ($|2^{(n+1)}\rangle$)) of the doublet. Some of these events will be radiative and hence, in this case, produce terahertz photons. Electroluminescence from similar Stark-ladder systems has been observed in the mid-infrared [14].

This view is reinforced by Fig. 3, which illustrates the electron energy-level structure for a section of a general N-well TASER at the operational bias point illustrated in Fig. 1(c). It can be seen that the two states localized in well n are supplemented by the ground state ($|1^{(n-1)}\rangle$) from well $n - 1$ and the first excited state ($|2^{(n+1)}\rangle$) to effectively form a four-level structure in each of the quantum wells. Note that an N-well superlattice will form $N - 2$ four-level structures. If the number of electrons in level $|2\rangle$ in any particular well could be made larger than the number of electrons in level $|1\rangle$, then the possibility of stimulated emission and gain will exist. Often (to zeroth order), electron scattering is inversely proportional to the energy separation between states; thus, the energy-level structure here indicated that the transition from $|2^{(n)}\rangle$ to $|1^{(n)}\rangle$ may be slower

placed at the center of the quantum well structure, then the states in the right-hand-well decrease in energy with respect to the states in the central well, and those in the left-hand-well increase. With the small ($\sim$20 meV) separation between the minibands, then it is inevitable (and, indeed, desirable in this

than $|1^{(n)}\rangle$ to $|2^{(n+1)}\rangle$ which are closely coupled, hinting at the possibility of a population inversion.

An edge-emitting TASER device would be constructed by incorporating a suitably designed superlattice in a metal-clad ridge waveguide [15]. Large oscillator strengths are achieved in this TASER by utilising terahertz radiation that is linearly polarized along the superlattice growth axis (z). Hence, in the waveguide, the terahertz radiation propagates in the fundamental TM mode. Fortunately, it is not necessary to use hundreds of periods in the waveguide TASER because the TM_0 mode will propagate even if the height of this TASER waveguide is only a small fraction of the THz wavelength, such as $\lambda/20$.

Note that this is a general design principle which is applicable to all mid- and far-infrared wavelengths. The wavelength of any radiative emission is determined by the separation of the ground and first excited states of the superlattice under bias; simply designing a structure around narrower quantum wells will allow the principle to be adapted to shorter wavelengths, though note that the shorter the wavelength, the larger the required bias to move the superlattice into the operating regime.

This superlattice device may resemble a Bloch oscillator in that in the present form it appears to be a long insulator region surrounded by n-type contacts, i.e., *niiiiiiiiiiiiiiiin*. It is well known that such structures are susceptible to nonuniform internal electric-field distributions and domain-formation which would jeopardize the device operation. However, quantum cascade lasers are similar structures, they are long, biased multiple-quantum-well systems, but they do not suffer from domain formation, and all the "active-region-injector" periods are equivalent. The reason is that the active (insulator) regions are separated by *doped* injectors; thus, the structure is a *ninininininin* structure. The ionised donors have the effect of shielding and pinning the electron distributions and help the field to stay uniform, and this could be utilized in the TASER suggested here—separate each active region of, say, 10 quantum wells by doped regions.

IV. THE CARRIER DYNAMICAL ISSUES

Although the system can be considered as a four-level laser, there are only two distinct levels, i.e., the ground (level 1) and first excited state (level 2) subbands, as illustrated in Fig. 3. The full laser energy-level structure is completed by states contributed from adjacent wells. The diagram shows the emission processes from each level with the lasing transition in well "n" denoted by the lifetime $\tau_{2(n)1(n)}$. Note that the lifetime includes contributions from phonon, electron-electron and radiative scattering, furthermore the reverse *absorption* process is also possible.

The number of electrons in any state could be described by a rate equation which consists of terms supplying electrons to that level and terms representing the removal of electrons from that level. In principle, in this system, electrons in any particular subband could scatter to the other subband in the same well (n), to both subbands originating from the well to the left ($n-1$) and both subbands originating from the well to the right ($n+1$).

Thus there will be five terms introducing electrons into any particular level (characterized by positive ($+$) coefficients) and five terms removing them (negative ($-$) coefficients). For the lasing ground state (level 1 in well n), the rate equation describing this would be

$$
\begin{aligned}
\frac{dn_1^{(n)}}{dt} = &+ \frac{n_{2(n+2)}}{\tau_{2(n+2)1(n)}} + \frac{n_{2(n+1)}}{\tau_{2(n+1)1(n)}} \\
&+ \frac{n_{2(n)}}{\tau_{2(n)1(n)}} + \frac{n_{1(n+1)}}{\tau_{1(n+1)1(n)}} \\
&+ \frac{n_{1(n-1)}}{\tau_{1(n-1)1(n)}} - \frac{n_{1(n)}}{\tau_{1(n)2(n+2)}} - \frac{n_{1(n)}}{\tau_{1(n)2(n+1)}} \\
&- \frac{n_{1(n)}}{\tau_{1(n)2(n)}} - \frac{n_{1(n)}}{\tau_{1(n)1(n+1)}} - \frac{n_{1(n)}}{\tau_{1(n)1(n-1)}}
\end{aligned} \tag{1}
$$

and similarly for the upper laser level

$$
\begin{aligned}
\frac{dn_2^{(n)}}{dt} = &+ \frac{n_{1(n-2)}}{\tau_{1(n-2)2(n)}} + \frac{n_{1(n-1)}}{\tau_{1(n-1)2(n)}} \\
&+ \frac{n_{1(n)}}{\tau_{1(n)2(n)}} + \frac{n_{2(n+1)}}{\tau_{2(n+1)2(n)}} \\
&+ \frac{n_{2(n-1)}}{\tau_{2(n-1)2(n)}} - \frac{n_{2(n)}}{\tau_{2(n)1(n-2)}} - \frac{n_{2(n)}}{\tau_{2(n)1(n-1)}} \\
&- \frac{n_{2(n)}}{\tau_{2(n)1(n)}} - \frac{n_{2(n)}}{\tau_{2(n)2(n+1)}} - \frac{n_{2(n)}}{\tau_{2(n)2(n-1)}}.
\end{aligned} \tag{2}
$$

At equilibrium, the rate of change of the population in any level (*with respect to time*) is clearly zero. Also, use can be made of the symmetry of the system: the number of electrons will be the same in each well; hence, the indices can be dropped on the subband populations, in addition there is a symmetry between the scattering rates, for example, $\tau_{1(n-1)1(n)} = \tau_{1(n)1(n+1)}$. Thus the above equation becomes

$$
\begin{aligned}
0 = &+ \frac{n_{2(n+2)}}{\tau_{2(n+2)1(n)}} + \frac{n_{2(n+1)}}{\tau_{2(n+1)1(n)}} + \frac{n_{2(n)}}{\tau_{2(n)1(n)}} \\
&- \frac{n_{1(n)}}{\tau_{1(n)2(n+2)}} - \frac{n_{1(n)}}{\tau_{1(n)2(n+1)}} - \frac{n_{1(n)}}{\tau_{1(n)2(n)}.}
\end{aligned} \tag{3}
$$

By analogy for the upper laser level

$$
\begin{aligned}
0 = &+ \frac{n_{1(n-2)}}{\tau_{1(n-2)2(n)}} + \frac{n_{1(n-1)}}{\tau_{1(n-1)2(n)}} + \frac{n_{1(n)}}{\tau_{1(n)2(n)}} \\
&- \frac{n_{2(n)}}{\tau_{2(n)1(n-2)}} - \frac{n_{2(n)}}{\tau_{2(n)1(n-1)}} - \frac{n_{2(n)}}{\tau_{2(n)1(n)}.}
\end{aligned} \tag{4}
$$

It appears at this point that there are two equations with two unknowns; however, all the carrier lifetimes τ_{if} depend on the subband populations in the initial "i" and final "f" states. Therefore, these two equations have to be solved self-consistently—this is achieved by following the method first mapped out in [16]. After an initial guess of the subband populations n_1 and n_2, all the lifetimes can be calculated by rearranging (3) into the form

$$
n_1 = \frac{\dfrac{n_2}{\tau_{2(n+2)1(n)}} + \dfrac{n_2}{\tau_{2(n+1)1(n)}} + \dfrac{n_2}{\tau_{2(n)1(n)}}}{\dfrac{1}{\tau_{1(n)2(n+2)}} + \dfrac{1}{\tau_{1(n)2(n+1)}} + \dfrac{1}{\tau_{1(n)2(n).}}} \tag{5}
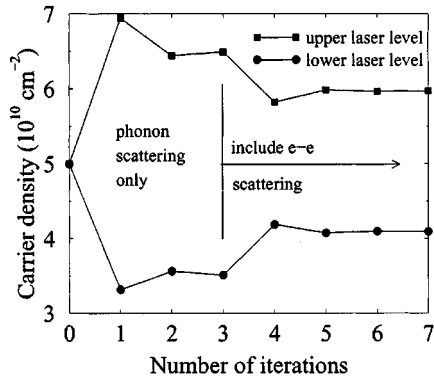$$

Fig. 4. Convergence of the subband carrier densities as a function of the number of iterations, note the initial populations were set equal at 5×10^{10} cm^{-2} and that for the first three iterations only phonon scattering was included. The particular example is the 240 Å GaAs/20 Å Ga$_{0.9}$Al$_{0.1}$As superlattice with a total carrier density of 10×10^{10} cm^{-2} per quantum well, at a field just beyond the anti-crossing (7.6 kVcm^{-1}) and at a temperature of 100 K.

It is postulated that this represents a better approximation to n_1 than the original guess. A similar equation can be derived for n_2 from (4)

$$n_2 = \frac{\dfrac{n_1}{\tau_{1(n-2)2(n)}} + \dfrac{n_1}{\tau_{1(n-1)2(n)}} + \dfrac{n_1}{\tau_{1(n)2(n)}}}{\dfrac{1}{\tau_{2(n)1(n-2)}} + \dfrac{1}{\tau_{2(n)1(n-1)}} + \dfrac{1}{\tau_{2(n)1(n)}}} \qquad (6)$$

The carrier lifetimes are then recalculated on the basis of these new populations and the procedure repeated until consistency is reached, i.e,. the point where the new estimates for n_1 and n_2 from (5) and (6) are the same as those found in the previous iteration. During the iteration, the subband populations are continuously renormalized in order to drive the solutions toward satisfying the total carrier density condition $n_1 + n_2 = N$.

In this work, the electron-longitudinal optic (LO) phonon and electron-electron scattering rates were included in the determination of all the lifetimes. The τ_{if} themselves are single numbers which represent the average lifetime of an electron to scattering between two subbands which each contain a thermalized Fermi-Dirac distribution [5]. For a comprehensive derivation and computer sourcecodes to repeat these calculations, see Harrison [17].

Fig. 4 shows the results of this iterative procedure for a particular superlattice design. The initial guess was chosen as equal electron populations of 5×10^{10} cm^{-2} in each of the six quantum well subbands in this three-well system (a total of 10×10^{10} cm^{-2} electrons per quantum well). For the first three iterations, in this and all subsequent calculations, only the electron-LO phonon emission and absorption processes were included for computational speed. For the latter iterations, electron–electron (e–e) scattering was introduced and this can be seen by the discontinuous change in the carrier densities in Fig. 4, *which also illustrates the importance of electron-electron scattering in intersubband systems.*

V. RESULTS AND DISCUSSION

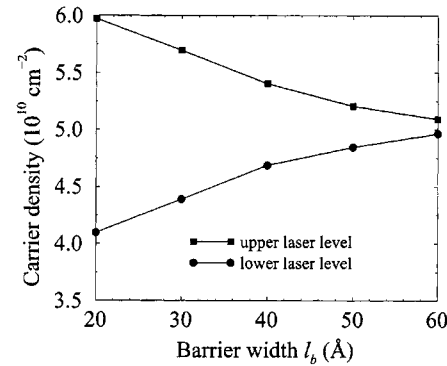Following some extensive numerical calculations, it was found that GaAs quantum wells of width 240 Å gave two

Fig. 5. Carrier densities in the upper and lower laser levels, at the optimum operating bias, as a function of the barrier width for a 240 Å GaAs/l_b Ga$_{0.9}$Al$_{0.1}$As superlattice at 100 K. Note the iterative procedure for $l_b = 20$ Å is the example given in Fig. 4.
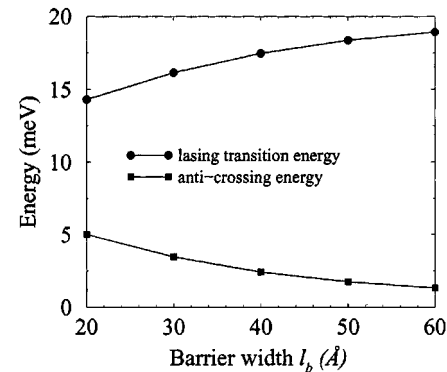

Fig. 6. Effect of the superlattice barrier width on the radiative transition energy and the anti-crossing energy of the same series of superlattices as in Fig. 5.

electron states separated by THz energies (4–41 meV) when surrounded by Ga$_{0.9}$Al$_{0.1}$As barriers. It was found that the first barrier width chosen (60 Å) gave a very small anti-crossing energy, which is used to depopulate the lower laser level and repopulate the upper laser level and this led to severe back scattering (phonon re-absorption), thus reducing the effectiveness of this scattering channel. Fig. 5 shows the results of further calculations: the barrier width was reduced from 60 to 20 Å with the aim of continued optimization. As the quantum well width was kept constant, the barrier width did effect the radiative energy, as can be seen in the upper curve of Fig. 6. However, the desired effect of *increasing* the anti-crossing energy, to reduce back scattering was achieved. Fig. 5 shows the beneficial effect of small barrier widths on the self-consistent electron densities in the upper ($|2^{(n)}\rangle$) and lower ($|1^{(n)}\rangle$) laser levels.

It can be seen that the initially poor population ratio of around 5% can be increased substantially to around 50% by narrowing the superlattice barrier width from 60 to 20 Å. More importantly, for laser gain the population difference is around 2×10^{10} cm^{-2} in this first series of calculations.

Taking the optimum structure from Fig. 5 of a 240 Å GaAs/20 Å Ga$_{0.9}$Al$_{0.1}$As superlattice, Fig. 7 shows the effect of temperature on the carrier densities. As might be expected for devices of this type, the population ratio decreases as the temperature increases, but it is still encouraging to note that there is still a population difference of $\sim 10^{10}$ cm^{-2} at room temperature.
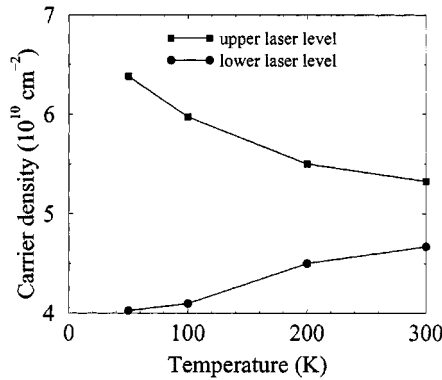
Fig. 7. Effect of temperature on the upper and lower laser level carrier densities in the 240 Å GaAs/20 Å $Ga_{0.9}Al_{0.1}As$ superlattice.
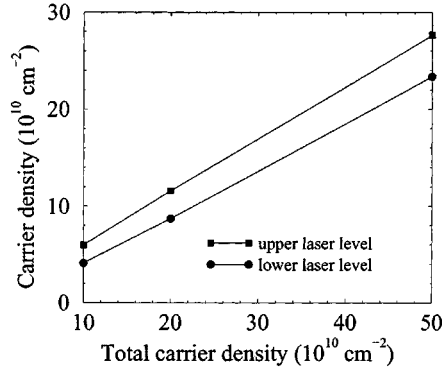

Fig. 8. Effect of total carrier density on the upper and lower laser level carrier densities in the 240 Å GaAs/20 Å $Ga_{0.9}Al_{0.1}As$ superlattice at 100 K.

Fig. 8 repeats the calculations for the structure of Fig. 7 for a range of total carrier densities in each quantum well for the fixed temperature of 100 K. It can be seen that although the population ratio decreases with increasing total carrier density (due to the increases in the electron-electron scattering), the population difference does increase. Again, this latter point is very encouraging for device realization.

VI. GAIN ESTIMATES

In addition to creating a population inversion, in order to make a laser it is also necessary to demonstrate gain within the lasing medium. Sun and Khurgin [18] give the gain (in cm^{-1}) of a four-level infrared intersubband laser as

$$g = \frac{4\pi e^2 |\langle 2|z|1 \rangle|^2 (N_2 - N_1)}{n\varepsilon_0 \lambda \hbar \Gamma} \qquad (7)$$

where

$(N_2 - N_1)$ volumetric population inversion (in cm^{-3});
n refractive index;
λ emission wavelength (in free space);
$\hbar\Gamma$ full-width at half-maximum (FWHM) of the stimulated emission.

Defining the quantum-well layer thickness as l_w, then the volumetric charge densities can be converted to the sheet charge densities (in cm^{-2}) used in this work, thus giving

$$g = \frac{4\pi e^2 |\langle 2|z|1 \rangle|^2 (n_2 - n_1)}{n\varepsilon_0 \lambda \hbar \Gamma l_w}. \qquad (8)$$

Taking the case of the 240 Å GaAs/20 Å $Ga_{0.9}Al_{0.1}As$ design, and the room temperature data point in Fig. 7, then $(n_2 - n_1) = 0.66 \times 10^{10} \ cm^{-2}$. Now, the dipole matrix element $\langle 2|z|1 \rangle$ for this design is 74 Å and the emission wavelength is $\lambda = 86.6 \ \mu m$, which implies a refractive index of about 3.3. Assuming the FWHM of the emission $\hbar\Gamma$ is 1 meV gives the gain as about $1200 \ cm^{-1}$, which is a quite substantial value. This is considerably higher than those measured for mid-infrared quantum cascade lasers (see for example [12]) and stems directly from the large dipole matrix element which comes from the use of a very wide quantum well in the active region.

VII. SUMMARY

A method of evaluating potential intersubband emitter device designs has been applied to a GaAs/$Ga_{1-x}Al_xAs$ implementation of a solid-state TASER. A self-consistent solution of the subband population rate equations, based on realistic evaluations of the intersubband scattering rates, has shown that the device design offers the potential for population inversion and significant population differences and gain at room temperature.

ACKNOWLEDGMENT

REFERENCES

[1] A. N. Korotkov, D. V. Averin, and K. K. Likharev, "Tasers—Possible dc pumped terahertz lasers using interwell transitions in semiconductor heterostructures," *Appl. Phys. Lett.*, vol. 65, p. 1865, 1994.
[2] G. Sun, Y. Lu, and J. B. Khurgin, "Valence intersubband lasers with inverted light-hole effective mass," *Appl. Phys. Lett.*, vol. 72, p. 1481, 1998.
[3] A. Liu and C. Z. Ning, "Terahertz optical gain based on intersubband transitions in optically pumped semiconductor quantum wells: Coherent pump-probe interactions," *Appl. Phys. Lett.*, vol. 75, p. 1207, 1999.
[4] K. Donovan, P. Harrison, and R. W. Kelsall, "Comparison of the quantum efficiencies of interwell and intrawell radiative transitions in quantum cascade lasers," *Appl. Phys. Lett.*, vol. 75, pp. 1999–2001, 1999.
[5] P. Harrison, "The nature of the electron distribution functions in quantum cascade lasers," *Appl. Phys. Lett.*, vol. 75, pp. 2800–2802, 1999.
[6] M. Rochat, J. Faist, M. Beck, U. Oesterle, and M. Ilegems, "Far-infrared ($\lambda = 88 \ \mu m$) electroluminescence in a quantum cascade structure," *Appl. Phys. Lett.*, vol. 73, p. 3724, 1998.
[7] B. S. Williams, B. Xu, Q. Hu, and M. R. Melloch, "Narrow-linewidth terahertz intersubband emission from three-level systems," *Appl. Phys. Lett.*, vol. 75, p. 2927, 1999.
[8] J. Ulrich, R. Zobl, K. Unterrainer, G. Strasser, and E. Gornik, "Magnetic-field-enhanced quantum-cascade emission," *Appl. Phys. Lett.*, vol. 76, p. 19, 1999.
[9] R. A. Soref, L. Friedman, G. Sun, M. J. Noble, and L. R. Ram-Mohan, "Quantum-well intersubband THz lasers and detectors," *SPIE Proc.*, vol. 3795, p. 516, 1999.
[10] K. Donovan, P. Harrison, and R. W. Kelsall, "Stark ladders as tunable far-infrared emitters," *J. Appl. Phys.*, vol. 84, pp. 5175–5179, 1998.
[11] R. F. Kazarinov and R. A. Suris, "Possibility of the amplification of electromagnetic waves in a semiconductor with a superlattice," *Sov. Phys.—Semiconduct.*, vol. 5, p. 707, 1971.
[12] C. Sirtori, P. Kruck, S. Barbieri, P. Collot, J. Nagle, M. Beck, J. Faist, and U. Oesterle, "GaAs/$Al_xGa_{1-x}As$ quantum cascade lasers," *Appl. Phys. Lett.*, vol. 73, p. 3486, 1998.
[13] S. Gianordoli, L. Hvozdara, G. Strasser, W. Schrenk, K. Unterrainer, and E. Gornik, "GaAs/AlGaAs-based microcylinder lasers emitting at 10 μm," *Appl. Phys. Lett.*, vol. 75, p. 1045, 1999.
[14] G. Scamarcio, F. Capasso, A. L. Hutchinson, D. L. Sivco, and A. Y. Cho, "Midinfrared emission from coupled wannier-stark ladders in semiconductor superlattices," *Phys. Rev. B*, vol. 57, p. R6811, 1998.

[15] A. Tredicucci, F. Capasso, C. Gmachl, D. L. Sivco, and A. Y. Cho, "Very long wavelength interminiband lasers," presented at the Materials Research Society Fall Mtg., Boston, MA, 1999.
[16] K. Donovan, P. Harrison, and R. W. Kelsall, "Self-consistent solution to the intersubband rate equations in quantum cascade lasers: Analysis of a GaAs/Al$_x$Ga$_{1-x}$As device," J. Appl. Phys., submitted for publication.
[17] P. Harrison, *Quantum Wells, Wires and Dots: Theoretical and Computational Physics*. New York: Wiley, 1999, p. 456.
[18] G. Sun and J. B. Khurgin, "Optically pumped four-level infrared laser based upon intersubband transitions in multiple quantum wells: Feasibility study," *IEEE J. Quantum Electron.*, vol. 29, p. 1104, 1993.

Paul Harrison (M'99–SM'99) received the B.Sc. degree from the University of Hull, Hull, U.K., and the Ph.D. degree from the University of Newcastle-upon-Tyne, Newcastle-upon-Tyne, U.K., in 1988 and 1991, respectively.

He was a postdoctoral Research Assistant at the University of Hull until 1995, when he obtained a Fellowship at The University of Leeds. Within the Institute of Microwaves and Photonics, he has been working on ways to adapt his theoretical and computational experience in semiconductor heterostructures to terahertz sources, and has recently been made "Reader in Quantum Electronics."

Richard A. Soref (S'58–M'63–SM'71) received the Ph.D. degree in electrical engineering from Stanford University, Stanford, CA, in 1963.

He served as a Staff Member at MIT Lincoln Laboratory, Cambridge, MA, during 1963–1965, and was a Member of the Technical Staff at Sperry Research Center, Sudbury, MA, from 1965 to 1983. In 1983, he joined the Air Force's Rome Air Development Center (now AFRL), Hanscom AFB, MA, where he is presently a Research Scientist in the Electromagnetics Technology Division of the Sensors Directorate. During these decades, he has contributed to electrooptical, guided-wave, and optical-microwave technology. Silicon-based optoelectronics, including quantum-well structures, has been his focus since 1986. He has authored or co-authored 180 journal articles and presentations, and has written six book chapters. Notable among his 24 invited talks are the 1998 lectures at the Fermi School in Varenna.. He holds 46 U.S. patents.

Since 1983, Dr. Soref has managed AFRL research contracts, and is active in OSA, IEEE, and MRS conference organization, serving recently as Chairman of the OSA's IPR-2000 Subcommittee on Dielectric Waveguides and as Co-Organizer of the Cross-connect Symposium. He was a Guest Editor of IEEE JOURNAL OF SELECTED TOPICS IN QUANTUM ELECTRONICS in 1998. He was awarded the U.S. Air Force Basic Research Award for pioneering work on semiconductor guided-wave optics in 1991, and is a Member of OSA, APS, MRS, SPIE, and a Fellow of AFRL.